

SEARCHING FOR THE MAIN POWERING OUTFLOW OBJECTS IN CEPHEUS A EAST

LUIS A. ZAPATA¹, MANUEL FERNÁNDEZ-LÓPEZ^{2,3}, SALVADOR CURIEL², NIMESH PATEL⁴, AND LUIS F. RODRÍGUEZ¹

To appear in the AJ

ABSTRACT

We present (sub)millimeter line and continuum observations in a mosaicing mode of the massive star forming region Cepheus A East made with the Submillimeter Array (SMA). Our mosaic covers a total area of about $3' \times 12'$ centered in the HW 2/3 region. For the first time, this observational study encloses a high angular resolution ($\sim 3''$) together with a large scale mapping of Cepheus A East. We report compact and high velocity $^{12}\text{CO}(2-1)$ emission associated with the multiple east-west bright H_2 condensations present in the region. Blueshifted and redshifted gas emission is found towards the east as well as west of HW 2/3. The observations suggest the presence of multiple large-scale east-west outflows that seems to be powered at smaller scales by radio sources associated with the young stars HW2, HW3c and HW3d. A kinematical study of part of the data suggests that the molecular outflow powered by HW2 is precessing with time as recently reported. Our data reveal five periodic ejections of material separated approximately every 10° as projected in the plane of the sky. The most recent ejections appear to move toward the plane of the sky. An energetic explosive event as the one that occurred in Orion BN/KL or DR21 does not explain the kinematics, and the dynamical times of the multiple ejections found here. The continuum observations only revealed a strong millimeter source associated with the HW 2/3 region. High angular resolution observations allow us to resolve this extended dusty object in only two compact sources (with spatial sizes of approximately 300 AU) associated with HW2 and HW3c. Finally, the bright optical/X-Ray HH 168 – GDD37 object might be produced by strong shocks related with the outflow from HW3c.

Subject headings: stars: formation — ISM: jets and outflows — ISM: individual objects (HW2, HW3c/d)

1. INTRODUCTION

Located at a distance of 700 pc (Moscadelli et al. 2009; Dzib et al. 2011), Cepheus A East is one of the nearest high-mass star formation regions. For this reason, Cepheus A East like Orion, is considered an ideal laboratory for the study of the physical processes related with the formation of the massive stars. This region has a total bolometric luminosity of about $2.5 \times 10^4 L_\odot$ (Evans et al. 1981). Half of this luminosity is attributed to the HW2 object, the brightest radio continuum source in the field, which is considered to be a B0.5 spectral type protostar (Rodríguez et al. 1994).

Cepheus A East contains a massive bipolar molecular outflow aligned primarily east-west (Rodríguez et al. 1980), but with additional components aligned northeast-southwest (Bally & Lane 1991; Torrelles et al. 1993; Gómez et al. 1999). The central $2'$ region contains high velocity as well as more compact extremely high velocity ^{12}CO components with radial velocities ranging from $+50$ to -70 km s^{-1} relative to the CO centroid (Narayanan & Walker 1996). The axis of the extremely high velocity outflow is rotated roughly 40° clockwise relative to the high velocity outflow on the plane of the sky. The smaller spatial extent together with the higher velocity suggests that the extremely high velocity flow traces a younger outflow component. At low velocities, there are additional blueshifted and redshifted components centered on HW2 that are oriented northeast-southwest.

This outflow complex also contains several Herbig-Haro

objects, including the extremely bright HH 168 or GGD 37 located about $100''$ due west of HW2, and several fainter bow shocks located to the east (Hartigan et al. 2000). Fainter HH objects (HH 169 and 174) are located in the eastern lobe (Hartigan et al. 2000). Pravdo & Tsuboi (2005) reported several distinct soft X-ray sources within the GGD 37 flow, one near the west, and one at the far end of the flow. They concluded that GGD 37 has a luminosity in X-Rays of $L_X = 3 \times 10^{30} \text{ erg s}^{-1}$, and inferred a shock velocity of 620 km s^{-1} for this object.

The complexity of the outflows, their multiple orientations and velocities, and the unclear morphology of some of the shock features make Cepheus A East challenging to interpret (Cunningham et al. 2009). However, the study of the kinematics, and morphology of the outflows ejected from the high-mass protostars located in Cepheus A East will allow us to understand better how the massive stars form in a clustered region.

Recent sensitive near-infrared H_2 line observations, and thermal infrared observations of this nearby massive star-forming region indicate that the massive young stellar object HW2 drives a pulsed, precessing jet that has changed its orientation by about 45° in roughly 10^4 years (Cunningham et al. 2009). This outflow thus appears to be responsible for most of the outflowing activity observed in Cepheus A. The precessing outflow is possibly feed by the massive and large dusty disk located in HW2 (Patel et al. 2005; Torrelles et al. 2007; Jiménez-Serra et al. 2009), and is associated with a bright and powerful radio thermal jet (Curiel et al. 2006; Rodríguez et al. 2005, 1994). Cunningham et al. (2009) proposed that the close passages of an intermediate mass companion through or near the circumstellar disk result in periods of enhanced accretion and mass loss, as well as forced precession of the disk. However, the presence of faint HH objects and molecular outflows with different orientations close to the HW2 object and

¹Centro de Radioastronomía y Astrofísica, Universidad Nacional Autónoma de México, Morelia 58090, México

²Instituto de Astronomía, Universidad Nacional Autónoma de México (UNAM), Apartado Postal 70-264, 04510 México, DF, México

³Astronomy Department, University of Illinois, 1002 West Green Street, Urbana, IL 61801, USA

⁴Harvard-Smithsonian Center for Astrophysics, 60 Garden Street, Cambridge, MA 02138, USA

towards the HH 168 object suggest that this precessing-jet model may not be the only mechanism working at this region to produce the outflowing activity.

At the moment, there have been only a few successful attempts to study the kinematics of this region after the pioneering single dish ^{12}CO single dish observations made by Rodríguez et al. (1980). Some examples include the extremely high angular resolution VLBI studies of water masers (Torrelles et al. 2011) which sample the kinematics only sparsely, due to the maser’s high selectivity, the proper motions measured in the radio jets present in this region (Rodríguez et al. 2005; Curiel et al. 2006), and the large scale SiO and HCO^+ maps from Gómez et al. (1999).

In the innermost parts of Cepheus A East there are multiple compact radio sources revealed mainly by sensitive Very Large Array (VLA) observations. For example, HW3 c/d are radio sources associated with a cluster of H_2O masers located at the core of this region. They are located $5''$ south of HW2 and close to the western end of a nearly continuous chain of radio sources along the southern rim of the Cepheus A East radio source complex.

Hughes & Wouterloot (1984) suggested that the bulk of the Cepheus A’s luminosity ($\sim 10^4 L_\odot$) likely arises from the radio sources HW2 and HW3 c/d that are associated with bright H_2O masers. However, no submillimeter continuum emission has been detected from HW3d, leading Brogan et al. (2007) conclude that HW3c is most likely to harbor the second most luminous and massive YSO in the Cepheus A East core. In this interpretation, radio source 3d may trace part of an elongated thermal jet from HW3c.

In this paper, we present high angular resolution (sub)millimeter continuum and line observations of the region Cepheus A East made with the Submillimeter Array⁵ (SMA). This is the first $^{12}\text{CO}(2-1)$ and submillimeter continuum study of Cepheus A East that contains a high angular resolution ($\sim 3''$) together with a large scale mapping ($3' \times 12'$). In Section 2, we discuss the observations made in this study. In Section 3, we present the data. In Section 4 we discuss the data, and in Section 5, we give the main conclusions.

2. OBSERVATIONS

2.1. Millimeter

The observations were made with the SMA on 2010 August 17th and 2010 October 17th, in its subcompact and compact configurations, respectively. The phase reference center for the observations was at $\alpha_{J2000.0} = 22^{\text{h}}55^{\text{m}}51^{\text{s}}.44$, $\delta_{J2000.0} = +62^\circ 01' 51''.3$. The frequency was centered at 220.53797 GHz in the Lower Sideband (LSB), while the Upper Sideband (USB) was centered at 230.53797 GHz. The primary beam of the SMA at around 230 GHz has a FWHM of about $50''$. We used the mosaicing mode with half-power point spacing between field centers and covered the entire Cepheus A East outflow region as far as it was mapped in H_2 by Cunningham et al. (2009), see Figure 1. We concatenated the two data sets using the task in MIRIAD called “*uvcat*”. The two different observations were identical, and only the antenna configuration of the SMA changed. The greatest angular size source that can be imaged on these observations is approximately $25''$ at a 10% level (Wilner & Welch 1994).

⁵ The Submillimeter Array (SMA) is a joint project between the Smithsonian Astrophysical Observatory and the Academia Sinica Institute of Astronomy and Astrophysics, and is funded by the Smithsonian Institution and the Academia Sinica.

The astrometric errors of these observations are about of $1''$.

The SMA digital correlator was configured in 24 spectral windows (“chunks”) of 104 MHz each, with 256 channels distributed over each spectral window, providing a resolution of 0.4062 MHz ($\sim 0.5 \text{ km s}^{-1}$) per channel. However, in this study, we smoothed the spectral resolution to about 1.5 km s^{-1} , because of the large width of the ^{12}CO line toward the Cepheus A East region (Rodríguez et al. 1980). The total bandwidth for both SMA observations is 8 GHz.

The zenith opacity ($\tau_{230\text{GHz}}$), measured with the NRAO tipping radiometer located at the Caltech Submillimeter Observatory, was from 0.2 to 0.05, indicating good weather conditions during the observations. Observations of Uranus provided the absolute scale for the flux density calibration. The gain phase calibrators were BLLAC, J2202+422, and J0014+612. The bandpass calibrator was the quasar 3C89. The uncertainty in the flux scale is estimated to be between 15 and 20%, based on the SMA monitoring of quasars. Further technical descriptions of the SMA, and its calibration schemes can found in Ho et al. (2004).

The data were calibrated using the IDL superset MIR, originally developed for the OVRO (Scoville et al. 1993) and adapted for the SMA⁶. The calibrated data were imaged and analyzed in the standard manner using the MIRIAD, AIPS, and KARMA (Gooch 1996) softwares. We set the ROBUST parameter of the task INVERT to +2 to obtain a slightly better sensitivity sacrificing some angular resolution. After concatenated the two data sets the resulting rms noise for the line images was around $150 \text{ mJy beam}^{-1}$ for each velocity channel (2 km s^{-1}) and 15 mJy for the continuum at an angular resolution of $3''.9 \times 3''.1$ with a P.A. = -11.6° . The $^{12}\text{CO}(2-1)$ line was detected at a frequency of about 230.5 GHz. Many more lines were detected in our spectral bands, however, most of them are associated with the compact object HW2 and do not with the multiple outflows emanating from this region. Thus, on this study, we only concentrated on the spatial distribution of the CO line emission. Moreover, even the compact emission from the SiO that is a natural outflow tracer is located only near HW2.

Here, we will assume a systemic velocity for the molecular cloud of -10 km s^{-1} as reported in Martín-Pintado et al. (2005).

2.2. Submillimeter

The observations were obtained from the SMA archive and were collected with 7 antennas of the SMA on 2005 November 30 in its very extended configuration. The receivers were tuned to a frequency of 341.0715 GHz in the USB, while the LSB was centered on 331.0715 GHz. The phase reference center for the observation was $\alpha_{J2000.0} = 22^{\text{h}}56^{\text{m}}17^{\text{s}}.98$, $\delta_{J2000.0} = +62^\circ 01' 47''.9$. The total bandwidth for this SMA observation is 4 GHz.

The zenith opacity ($\tau_{230\text{GHz}}$) was about 0.06, indicating excellent weather conditions. Observations of Ceres provided the absolute scale for the flux density calibration. The uncertainty in the flux scale is estimated to be again between 15 and 20%. The gain phase calibrator was the quasar BLLAC. The bandpass for this observation was the quasar 3C454.3. The continuum rms noise was around 15 mJy beam^{-1} at an angular resolution of $0''.74 \times 0''.73$ with a P.A. = 32.7° . The data was self-calibrated in phase and amplitude.

⁶ The MIR-IDL cookbook by C. Qi can be found at <http://cfa-www.harvard.edu/~cqi/mircook.html>

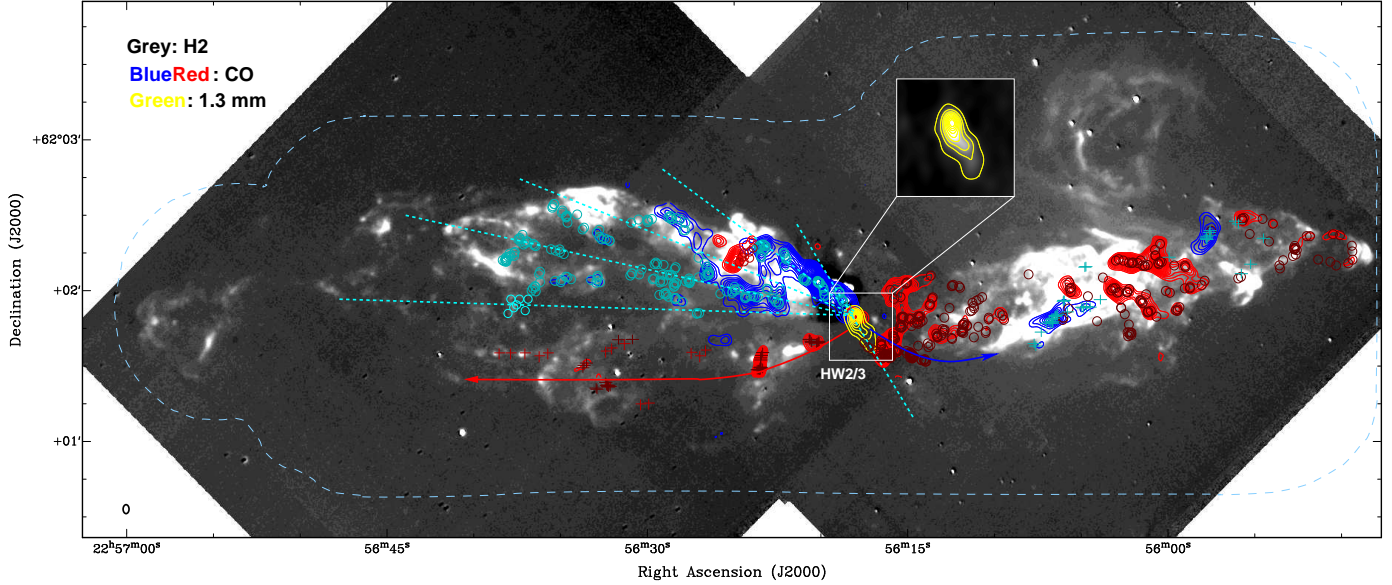


FIG. 1.— Integrated intensity contour map of the $^{12}\text{CO}(2-1)$ emission overlaid on the H_2 image presented in Cunningham et al. (2009). The redshifted and blueshifted emission are represented by red and blue contours, respectively. The blue and red contours start from 10% to 90% with steps of 3% of the peak of the molecular emission; the peak of the line map is $85 \text{ Jy beam}^{-1} \text{ km s}^{-1}$ for the blueshifted gas and $75 \text{ Jy beam}^{-1} \text{ km s}^{-1}$ for the redshifted gas. The range for the integrated redshifted emission is from $+5$ to $+55 \text{ km s}^{-1}$, while the range for the integrated blueshifted emission is from -65 to -14 km s^{-1} . The systemic velocity assumed here is -10 km s^{-1} . The yellow contours represent the 1.3 mm continuum emission. The yellow contours are from +10% to 90% with steps of 10% of the peak of the emission; the peak of the continuum map is 1.0 Jy beam^{-1} . Additionally, the blue/red circles and crosses mark the position of the ^{12}CO emission condensations found at different velocity channels. The ^{12}CO emission close to the systemic velocity was poorly sampled with the SMA and is not presented in this image. The open circles trace emission likely arising from HW2, while the crosses trace the emission arising from the HW3 region (see text). The continued and dashed lines mark the orientations of the outflows emanating from HW2 and HW3, respectively. The blue dashed line at the edge of the H_2 image marks the area that our SMA mosaic covers. The synthesized beam of the line and continuum observations is shown in the lower left corner. The inset in the image shows a zoom toward the continuum millimeter source reported here.

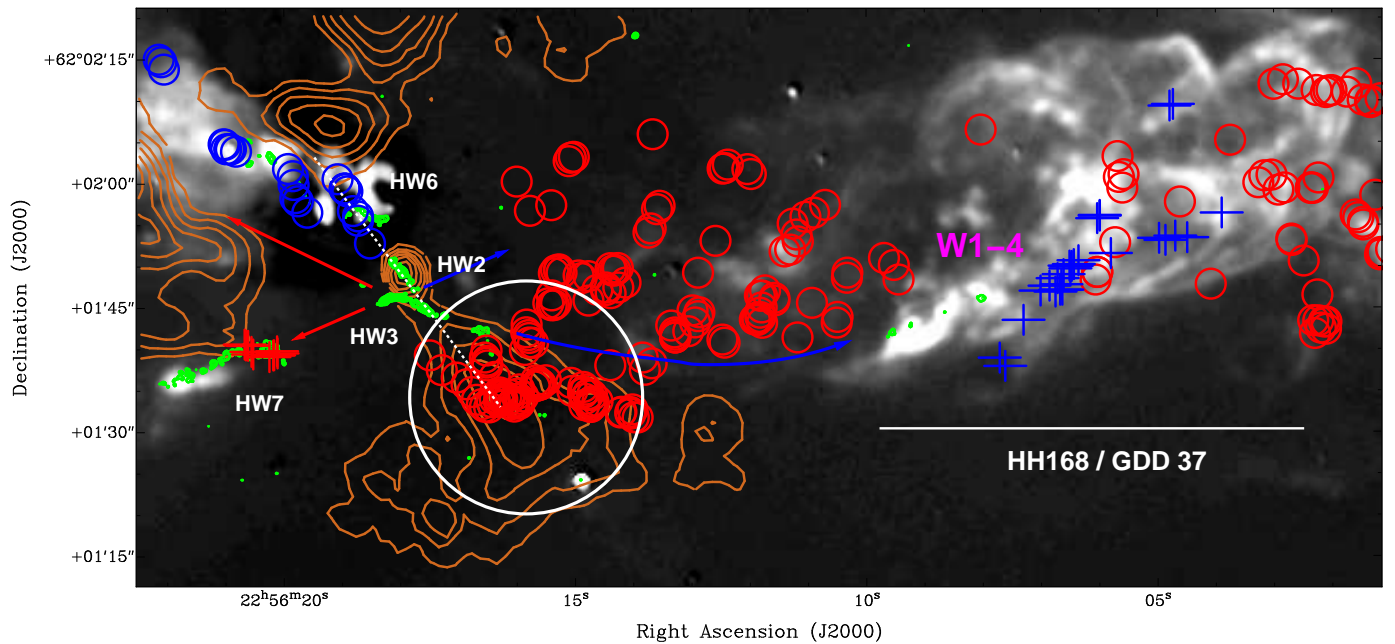


FIG. 2.— Zoom into the HW2 / HW3, and the HH 168 regions. As in the case of Figure 1, the blue and red open circles/crosses mark the position of the ^{12}CO emission peaks at different velocity channels, and are overlaid on an H_2 image. The green contours trace the VLA radio emission (Curiel et al. 2006; Rodríguez et al. 1994). The green contours are from +5% to 90% with steps of 1% of the peak of the emission; the peak of the continuum map is $4.0 \text{ mJy beam}^{-1}$. The brown contours trace the $\text{NH}_3(1,1)$ emission (Torrelles et al. 1993). The physical and observational parameters of these NH_3 condensations are given in Torrelles et al. (1993). The brown contours start from 15% to 90% with steps of 10% the peak of the molecular emission; the peak of the line map is $257 \text{ Jy beam}^{-1} \text{ km s}^{-1}$. The white circle marks the position of the "shocked-zone" described in the text.

3. RESULTS

3.1. Millimeter continuum emission

In Figure 1, we show the resulting 1.3 mm. continuum image from the Cepheus A East from our SMA observations. The continuum emission is represented by yellow contours in this Figure. The mosaic covered a total area of about $3' \times 12'$ centered at the HW 2/3 region. We only detected a strong and compact source associated with HW 2/3. The source has additionally a small tail that extends to the southwest by a few arcseconds. A similar morphology was already reported by Brogan et al. (2007). The physical and observational parameters of this source are presented in Table 1. The compact millimeter source is coincident with a strong and compact condensation of NH_3 associated with HW2, see Figure 2. The physical and observational values for this compact NH_3 condensation are given in Torrelles et al. (1993).

Following to Zapata et al. (2012) and assuming a dust temperature of 50 K, a distance of 700 pc, a $\beta = 1.5$, optically thin and isothermal dust emission, and a gas-to-dust ratio of 100, we found a dust-mass detection 4σ limit of $0.5 M_\odot$. This suggests that the presence of a cluster of young very low-mass stars might be present in Cepheus A East.

3.2. Submillimeter continuum emission

In Figures 3 and 4, we show the submillimeter continuum maps obtained with the SMA. We found submillimeter compact continuum emission associated with only two objects, HW2 and HW3c. This is in agreement with the submillimeter maps presented in Brogan et al. (2007). However, in their maps they found a very faint source called SMA4 that is not detected here at a 4σ level. Both maps, the presented here and that obtained by Brogan et al. (2007), have similar rms-noises so that we believe that such differences could come from the different *uv-coverage* obtained in the observations. The observational and physical parameters of these sources are given in Table 1. The millimeter source associated with HW3c is not resolved. The values for the fluxes obtained here from both sources (HW2 and HW3) are also in good agreement with the values obtained in Brogan et al. (2007). To obtain the physical dimensions and flux densities of the continuum sources we used the task *imfit* of the MIRIAD. This routine uses gaussian fitting to derive these parameters.

3.3. $^{12}\text{CO}(2-1)$ line emission

In Figure 1, we show the main results of the line emission analysis. In this image, we present the integrated intensity of the line emission (moment zero map) together with the position of each gas compact condensation found in our spectral channel maps. This figure is made in this way because the dominant parts of the outflow do not allow us to see clearly fainter molecular gas in our moment zero map. This effect is clearer far from the center of the image, where the ^{12}CO line emission is mainly extended and faint. The blue and red contours represent the ^{12}CO gas emission that is approaching and receding from us, respectively. Receding (redshifted) ^{12}CO features show radial velocities down to 65 km s^{-1} while the approaching molecular ^{12}CO gas has values up to -55 km s^{-1} . The moment zero map is overlaid with the H_2 emission, which is related with shocked gas and is presented in Cunningham et al. (2009). It is evident that there is a good alignment between the ^{12}CO and H_2 emission. In both sides of the outflow redshifted and blueshifted gas is found, suggesting the presence of multiple outflows with different ori-

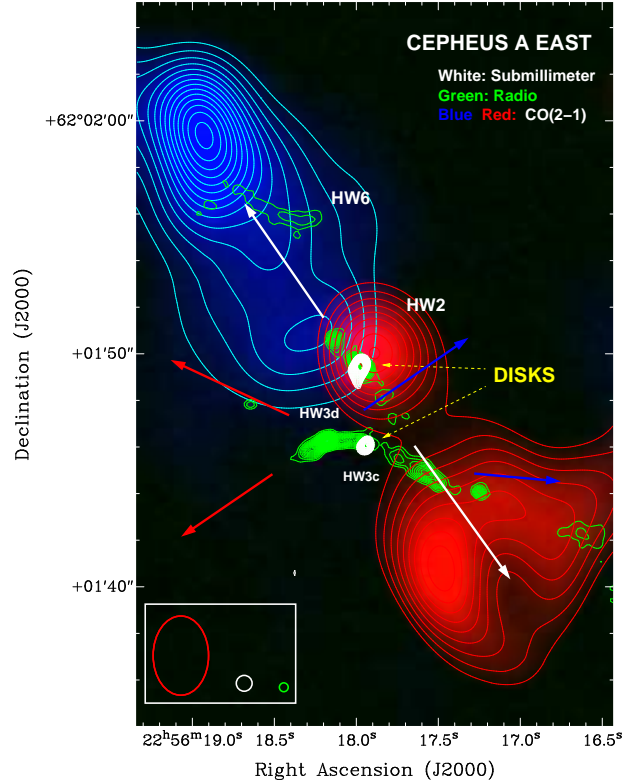


FIG. 3.— Integrated intensity color and contour maps of the $^{12}\text{CO}(2-1)$ emission from the HW 2/3 region overlaid in contours with the SMA $890 \mu\text{m}$ continuum emission (white) and the VLA 6 cm continuum emission (green). The blue and red contours are from 30% to 90% with steps of 10% of the peak of the line emission; the peak of the $^{12}\text{CO}(2-1)$ emission is $24 \text{ Jy beam}^{-1} \text{ km s}^{-1}$ for the blueshifted gas and $18 \text{ Jy beam}^{-1} \text{ km s}^{-1}$ for the redshifted gas. The integration range for the blueshifted velocities was -22 km s^{-1} to -19 km s^{-1} , while for the redshifted velocities was -4 km s^{-1} to -1 km s^{-1} . The systemic velocity assumed here is -10 km s^{-1} . The white contours are from 40% to 90% with steps of 5% of the peak of the emission; the peak of the $890 \mu\text{m}$ map is $420 \text{ mJy beam}^{-1}$. The green contours are from 10% to 90% with steps of 3% of the peak of the emission; the peak at 6 cm is $4.0 \text{ mJy beam}^{-1}$. The synthesized beams of the line and continuum observations are shown in the bottom left corner. The white, blue, and red arrows represent the orientation of the multiple outflows emanating from this region. The molecular emission extending outside of the figure is associated with multiple east-west outflows.

entations emanating from the HW 2/3 region. Figure 1 only displays the most prominent ^{12}CO emission features detected outside of the velocity window -13 to -4 km s^{-1} . Within this window the radiation stems predominantly from the ambient cloud and is spatially extended, thus cannot be properly reconstructed by the SMA. On the other hand, the emission at high velocities is generally compact (e.g. Rodríguez-Franco et al. 1999), and is properly reconstructed by the SMA, see for example the outflow located in Orion-KL (Peng et al. 2012). Here, we take as compact emission, ^{12}CO molecular structures with sizes of about two or three synthesized beams.

In Figures 1 and 2, we have distinguished the molecular material ejected by HW2 and HW3c/d with blue and red open circles for HW2 and blue and red crosses for HW3c/d. We are able to do this because of the different orientations of the molecular outflows. For example, the redshifted and blueshifted emission for the outflow from HW2 is mostly located in the west and east, respectively. The outflow powered by HW3c approximately has its redshifted side in the northeast and its blueshifted side in the west.

In Figures 3 and 4, we show ^{12}CO moment zero maps

TABLE 1
PARAMETERS OF THE SMA (SUB)MILLIMETER SOURCES

Source	Position		Flux Density (mJy)	Deconvolved size ^a			Mass (M_{\odot})
	α_{2000} (h m s)	δ_{2000} ($^{\circ}$ ' ")		Maj. (")	Min. (")	P.A. ($^{\circ}$)	
HW2/3	22 56 17.999	+62 01 48.82	2.1 ± 0.3	5.3 ± 0.5	0.7 ± 0.2	-13.1	5
HW2	22 56 17.978	+62 01 49.39	0.9 ± 0.2	0.77 ± 0.05	0.3 ± 0.1	-152	0.5
HW3c	22 56 17.943	+62 01 46.04	0.4 ± 0.2	—	—	—	0.3

NOTE. — (a): These values were obtained from the task IMFIT of MIRIAD.

using a limited velocity window, trying therefore to reveal young molecular gas (or gas that is closer to the exciting sources as compared to the most eastern gas) associated with HW2 and HW3. Both maps show bipolar collimated outflows emanating from each of these sources. The molecular outflows appear to emanate from the compact submillimeter and radio sources associated with HW2, HW3d, and HW3c. At very small scales (about 2000 AU) and in the middle of the flows, it is found the compact radio emission reported by Curiel et al. (2006); Rodríguez et al. (1994). The radio emission associated with HW2 is related to a powerful radio thermal jet with tangential velocities of about 500 km s^{-1} (Curiel et al. 2006). The nature of the radio emission associated with HW3c/d, on the other hand, is still unknown. However, their spectral indices and morphologies are consistent with possible thermal jets with different orientations (Garay et al. 1996; Chibueze et al. 2012). No clear proper motions of the ionized gas are observed toward these sources (Rodríguez et al. 2005). Here, we assume that these sources are in fact extended thermal jets, however, more observations are still needed to confirm this hypothesis.

For the case of HW2, the redshifted emission is found in the southwest while blueshifted emission is in the northeast. For HW3c, the redshifted emission is found to the east while blueshifted emission is in the west (see Figure 4). There is some redshifted emission located in northeast of HW2/3 region (Figure 1), maybe this is part of this bipolar outflow powered by HW3c. For HW3d, we think that the redshifted emission found to the southeast (towards HW7) is related with this object, but there is no evidence from our observations of blueshifted emission towards the northwest, probably because the blueshifted outflowing material goes directly outside of the molecular cloud as it seems to be case in some others molecular outflows (Chernin & Masson 1995; Zapata et al. 2010). This picture is consistent with the SE-NW outflow traced by the water proper motions, and the orientation of the thermal jet reported by Chibueze et al. (2012) in HW3d.

The small changes observed in the orientation of the different outflows found in Cepheus A east can be explained by the outflows undergoing deflections, possibly due to the high density molecular cloud. A process for the deflection of an outflow has been proposed and modeled by Raga & Canto (1995). However, again many more observations and theoretical studies are still needed to confirm this proposition.

The ^{12}CO emission arising from these outflows is also associated with H_2 and radio emission located far from the energizing sources (e.g. the zone close to HW7 and HW6). This radio emission is probably produced by strong shocks in dense zones (Rodríguez et al. 2005).

The orientation of the outflows reported here are in agreement with the position of the multiple outflows emanating from this region proposed by Goetz et al. (1998), see their

Figure 7.

4. DISCUSSION

4.1. Dusty Envelope and Circumstellar Disks

Following Zapata et al. (2012), we adopted a value of $\kappa_{1.3\text{mm}} = 0.1 \text{ cm}^2 \text{ g}^{-1}$ (Ossenkopf & Henning 1994) and assumed optically thin, isothermal dust emission, a distance to Cepheus A East of 700 pc (Moscadelli et al. 2009; Dzib et al. 2011) and a gas-to-dust ratio of 100, with a dust temperature of 50 K for the extended millimeter object associated with HW 2/3, deriving a dust mass of 5 solar masses. At these wavelengths, the emission from the ionized jets is negligible because its emission depends on frequency as $\nu^{0.6}$ (Reynolds 1986). The mass and linear sizes ($\sim 2000 \text{ AU}$) suggest that this dusty source (shown in Figure 1) is likely a large envelope surrounding the compact objects HW2 and HW3.

For the case of the submillimeter compact sources, we found masses of about $0.5 M_{\odot}$. We assumed a dust temperature of 100 K, and a dust opacity of $\kappa_{0.8\text{mm}} = 0.15 \text{ cm}^2 \text{ g}^{-1}$. The mass and linear size ($\sim 350 \text{ AU}$) of HW2 are consistent with the values obtained for the circumstellar disk reported by Patel et al. (2005); Torrelles et al. (2007); Jiménez-Serra et al. (2009). However, the circumstellar disk could be not only forming a single massive star (Curiel et al. 2002; Comito et al. 2007; Brogan et al. 2007). For the case of HW3c, we suggested that the dusty object mapped here and shown in Figure 3 is also a circumstellar disk that powers the east-west bipolar outflow shown in Figure 4. A more compressive discussion about this hypothesis will give in a future paper (Curiel et al. 2013).

4.2. Molecular Outflows

4.2.1. The pulsed and precessing outflow from HW2

We found strong and compact molecular ^{12}CO line emission associated with the pulsed and precessing outflow reported by Cunningham et al. (2009). The redshifted emission is found to the west while the blueshifted is found to the east. The blueshifted emission is mostly distributed in compact condensations that follow well the H_2 emission. Very close to HW2 well defined jet-like structures are observed. The redshifted emission, on the other hand, is distributed regularly forming arcs with different orientations and sizes. Most of the molecular arcs are formed on the tips of the H_2 bow shocks. We found ^{12}CO blueshifted and redshifted emission at distances up to 1 pc away from HW2. We do not detect ^{12}CO emission from the most eastern H_2 bow shock (HH 174). From our data it is not clear whether the object HH 174 was ejected from HW2 as suggested by Cunningham et al. (2009), or maybe this was produced by HW3c/d long time ago. Most of ^{12}CO emission detected by Rodríguez et al. (1980) and Cunningham et al. (2009) using single dishes, seems to be

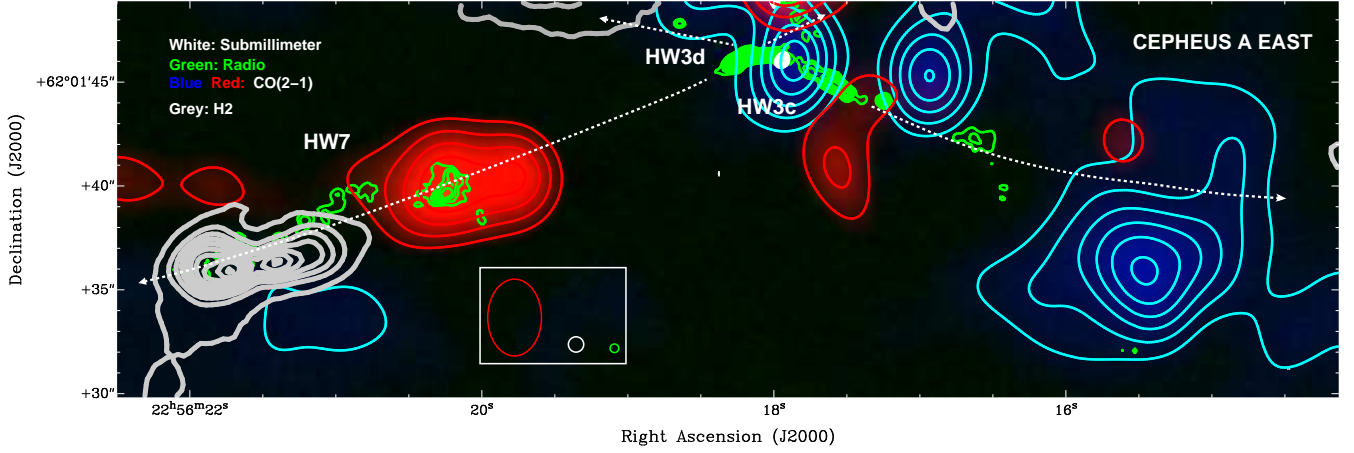


FIG. 4.— Integrated intensity color and contour maps of the $^{12}\text{CO}(2-1)$ emission from the HW3 region overlaid in contours with the SMA $890\ \mu\text{m}$ continuum emission (white), infrared H_2 emission (grey) and the VLA 6 cm continuum emission (green). The blue and red contours are from 40% to 90% with steps of 10% of the peak of the line emission; the peak of the $^{12}\text{CO}(2-1)$ emission is $17\ \text{Jy beam}^{-1}\ \text{km s}^{-1}$ for the redshifted gas, and $12\ \text{Jy beam}^{-1}\ \text{km s}^{-1}$ for the blueshifted gas. The integration range for the blueshifted velocities was $-17\ \text{km s}^{-1}$ to $-14\ \text{km s}^{-1}$, while for the redshifted velocities was $-7\ \text{km s}^{-1}$ to $-4\ \text{km s}^{-1}$. The systemic velocity assumed here is $-10\ \text{km s}^{-1}$. The white contours are from 40% to 90% with steps of 5% of the peak of the emission; the peak of the $890\ \mu\text{m}$ map is $420\ \text{mJy beam}^{-1}$. The green contours are from 10% to 90% with steps of 3% of the peak of the emission; the peak at 6 cm is $4.0\ \text{mJy beam}^{-1}$. The synthesized beams of the line and continuum observations are shown in the lower left-middle corner. The white arrows represent the orientation of the multiple outflows emanating from this region.

extended and was likely resolved out in our high resolution maps.

From our ^{12}CO map, presented in Figure 1, it is not easy to see the eastern ejections formed at different angles of the precessing outflow driving by HW2 and reported by Cunningham et al. (2009). This is only clear near HW2. The emission is mostly concentrated in small groups dispersed across the H_2 bow shocks. In Figure 5, we show a part of the velocity cube obtained here trying to illustrate how we get the physical information of each compact condensation present in our SMA data. If we plot the position angle vs. the projected distance with respect to the position of HW2 of each ^{12}CO condensation found in our spectral channel cube (see Figure 6), one can distinguish groups of condensations separated approximately every 10° . This result is in very good agreement with that reported by Cunningham et al. (2009) and that is shown in our Figure 1. In a first approximation, the condensations with small position angles are close to HW2, while the condensations with large angles are far from HW2. This is also the case for the west side of the outflow (see Figure 5). For example, condensations that have PAs between 40° to 60° are located in a range of $10''$ to $20''$ from HW2 (very close of this object), in the other hand, condensations with PAs about 93° are far from HW2, about $250''$. However, there are some condensations that show a large spread of distances in a small range of angles. These condensations have an average angle of 85° and are associated with a single ejection from HW2. The small differences between both diagrams (Figures 5 and 6) are probably due to inhomogeneities of the molecular cloud.

In Figure 7, we show a similar diagram to that made in Figure 6, but now plotting the average position angles vs. the average radial velocities of the ^{12}CO compact condensations. These average radial velocities are obtained averaging the radial velocities of each condensation that are inside of the dashed box presented in Figure 6. In this way, for one average angle in the dashed box, we have a average radial velocity. This plot reveals that the recent ejections of the outflow in average have small position angles and small radial velocities, suggesting that the outflow is thus approaching to the plane

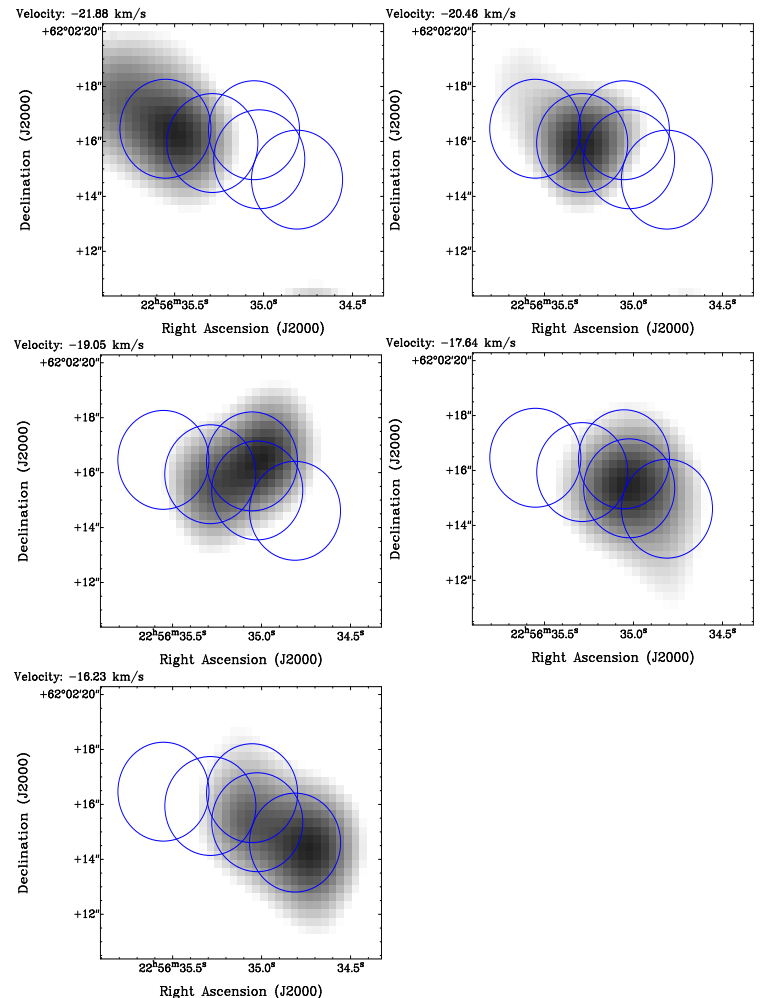


FIG. 5.— A part of the velocity cube for a single blueshifted filament showing how the physical information of each filament using a gaussian fitting was obtained. Note that approximately the size of every molecular condensation is about one beam. The blue circles mark the position of the condensations.

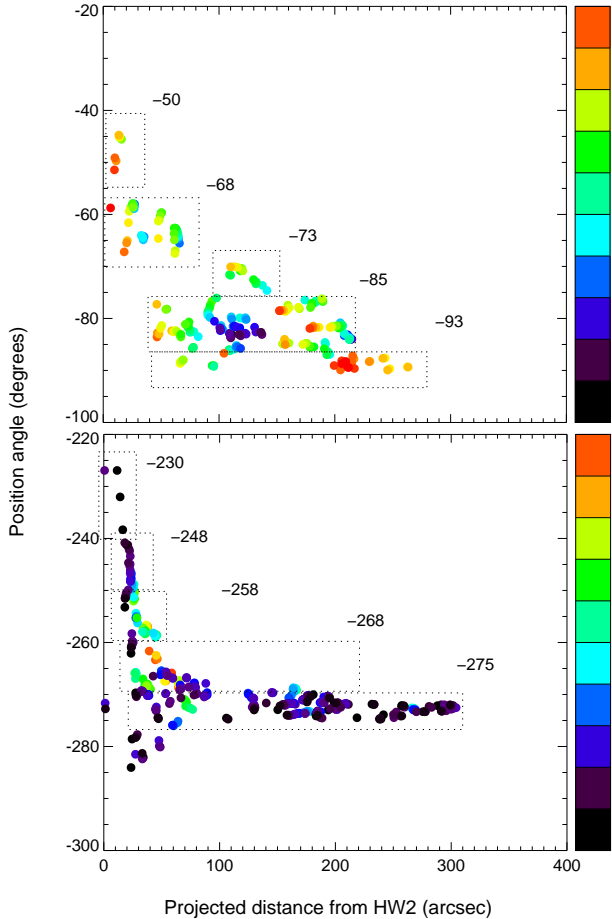


FIG. 6.— Position angle vs. projected distance to HW2 digram for the blueshifted and redshifted ^{12}CO spots. The ^{12}CO spots are additionally color-coded to their respective radial velocities. The dashed boxes show the groups of ^{12}CO condensations for different position angles.

of the sky at present. The past ejections in average have large position angles and large radial velocities indicating that the outflow in the near past was probably located perpendicular to the plane of the sky. However, the condensations with the largest radial velocities also show low radial velocities. This suggests that maybe long time ago the outflow was ejecting material close to the plane of the sky as it is doing now.

Our plots revealed only five ejections separated by about 10° , one more than Cunningham et al. (2009). As mentioned earlier, from our data it is not clear that the object HH 174 was ejected from HW2. We found very high velocity molecular gas associated with HW2 that is not presented in our Figures 5 and 6, but either this is presented in our moment zero map (Figure 1). For example, in our Figure 5, this emission represents a single multicolor point in the $(0,0)$ position that does not contribute to our findings. Perhaps this high velocity material is part of very new ejections of HW2 with high velocity. The present size and orientation of the molecular outflow is shown in Figure 3. The present orientation of the outflow coincides very well with that of the powerful thermal jet (Curiel et al. 2006; Rodríguez et al. 1994).

In Figure 8, we show the kinematics of the molecular gas associated with the precessing outflow powered by HW2. This position-velocity diagram reveals that the kinematics of the multiple flows is very different of that observed in the

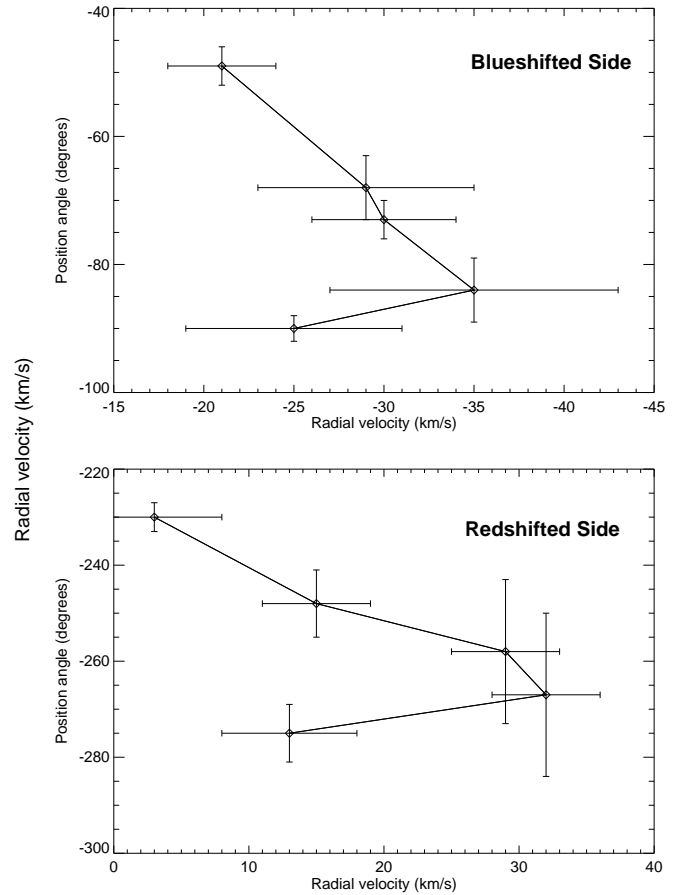


FIG. 7.— Similar plot as the one presented in Figure 5, but only averaging the ^{12}CO condensations in different groups of position angles. The average velocity and position values show their respective error bars. The error bars are the standard error on the mean. The edges of the bins here are an approximation trying to select the molecular condensations in groups of 10° .

explosive outflow in Orion BN/KL and DR21 (Zapata et al. 2009, 2011, 2013). The molecular condensations from the precessing outflow mostly stay around some place with respect to a range of velocities and show large velocity gradients, contrary to the Hubble Law observed in the molecular filaments arising from Orion BN/KL or DR21, see Figures 2 of Zapata et al. (2009, 2013). In the case of Orion BN/KL and DR21, the molecular condensations move in position when the velocity change, following a linear correlation between velocity and position. In conclusion, we suggest that an energetic explosive event as the one occurred in Orion BN/KL does not explain the kinematics of the multiple molecular outflows found here. The kinematics of the molecular ejections observed in the CepA HW2/3 region is better explained by the presence of a precessing outflow.

From Figure 8, it is clear that the ^{12}CO line emission with the largest redshifted line widths are located close to HW2 and from Figure 2 one can see that it coincides with a high density ammonia core. We have marked this region with a circle in Figure 2. We think that this high density region might be blocking part of the redshifted side of the molecular outflow creating a "shocked zone". This "shocked zone" could explain why it is not observed the redshifted bow shocks with similar position angles as the blueshifted bow shocks if both sides come from the same precessing bipolar outflow. We re-

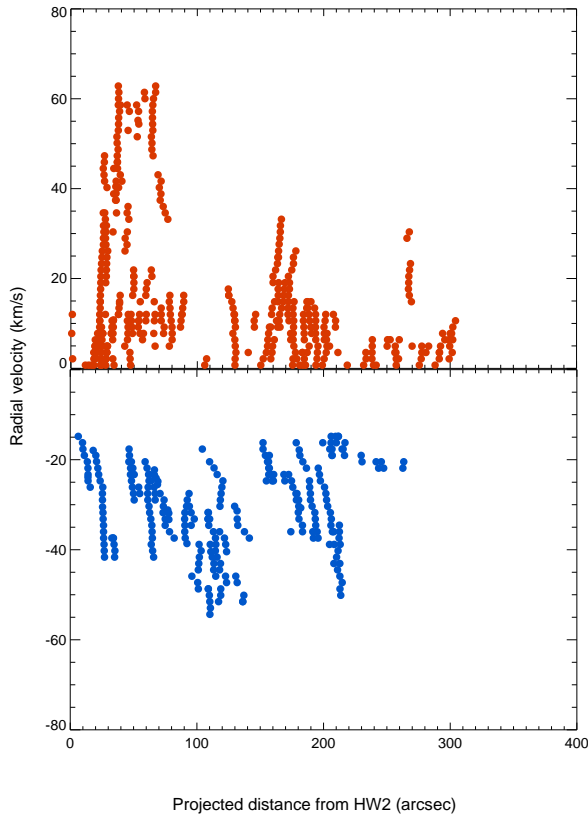


FIG. 8.— Position-velocity relation of the $^{12}\text{CO}(2-1)$ structures from HW2: radial velocity as a function of on-the-sky distance from the position of HW2. Note that velocities between -13 and 0 km s^{-1} could not be investigated because of interferometric contamination with the extended molecular gas.

fer again to the readers see Torrelles et al. (1993) for the physical values of this ammonia condensation.

4.2.2. The bipolar outflows from HW3c/d

Our observations revealed the presence of two east-west low-velocity bipolar outflows that are emanating from HW3c/d. The innermost parts of the outflows appear to be traced by elongated ionized thermal jets reported by Garay et al. (1996); Rodríguez et al. (1994, 2005) (see Figure 4). The outflow powered by HW3d appears to be creating the zone called HW7 located to the southeast and forming some more eastern HH objects far from HW3. The proper motions of HW7 are complex, however, Rodríguez et al. (2005) suggested that they are being produced by a source to its northwest, perhaps by HW3. This is in good agreement to what we propose here based on our ^{12}CO observations. On the other hand, the blueshifted side of the outflow powered by HW3c goes to the west and seems to connect with the optical/X-Ray object, known as the HH 168 or GDD 37 (Pravdo et al. 2009; Schneider et al. 2009a,b; Hartigan et al. 2000, 1986). HH 168 is also blueshifted (Hiriart et al. 2004).

There is also the possibility that the radio objects W1-4 (Rodríguez et al. 2005) are also energized by the blueshifted side of the outflow from HW3c, however, their radial velocities are still unknown. These objects show westward proper motions in the range of 120 to 280 km s^{-1} . Rodríguez et al. (2005) proposed that these radio objects are energized by HW3.

Chibueze et al. (2012) proposed that the object HW3d harbors an internal massive young star that powers a NW-SE water maser outflow and the thermal radio jet. This source could be energizing the object HW7 and perhaps the most eastern HH objects as mentioned before. However, we do not find any submillimeter continuum emission associated with this source. Perhaps this source is associated with a lower mass young stellar object and more sensitive millimeter observations are needed to reveal the dust emission associated to this protostar.

5. SUMMARY

We have observed the Cepheus A East region using the Submillimeter Array. We made (sub)millimeter line and continuum observations in a mosaicing mode of this massive star forming region. Our mosaic covers a total area of about $3' \times 12'$, centered in the HW 2/3 region. Our main conclusions are as follows:

- We report compact and high velocity $^{12}\text{CO}(2-1)$ emission associated with the multiple east-west H_2 bow shocks present in Cepheus A East. Blueshifted and redshifted gas emission is found towards the east as well as to the west from HW2. Receding ^{12}CO features show radial velocities up to 65 km s^{-1} while the approaching ^{12}CO line emission has velocities down to -55 km s^{-1} .
- The $^{12}\text{CO}(2-1)$ observations suggest the presence of three large-scale east-west outflows, likely powered at small scales by the radio sources associated with the young massive protostars HW2, HW3c and HW3d.
- We confirm the precession associated with the molecular outflow powered by HW2. Our data reveal five periodic ejections of material separated approximately every 10° . There is some evidence that this outflow had an orientation perpendicular to the plane of the sky on the past.
- An energetic explosive event as the one that occurred in Orion BN/KL or DR21 does not explain the kinematics of the multiple molecular outflows found here.
- In our entire field, the continuum observations only revealed a strong millimeter source associated with the HW 2/3 region. We resolved this extended dusty object in only two compact sources associated with HW2 and HW3c. These compact objects are tracing the circumstellar disks associated with these objects.
- The bright optical/X-Ray HH 168 object might be produced by strong shocks with the molecular cloud and arising from the outflow energized by HW3c.

In conclusion, the bipolar flows arising from HW2 and HW3c/d might explain the whole outflow activity observed in Cepheus A East. However, many more observations at different wavelengths are needed to confirm this hypothesis. In particular, future observations using other molecular species may reveal more outflows in this high-mass forming region.

L.A.Z., L.F.R. and S.C. acknowledge the financial support from DGAPA, UNAM, and CONACyT, México. We are very grateful to John Bally for having provided the H_2 image.

REFERENCES

- Bally, J., & Lane, A. P. 1991, *Astronomical Society of the Pacific Conference Series*, 14, 273
- Brogan, C. L., Chandler, C. J., Hunter, T. R., Shirley, Y. L., & Sarma, A. P. 2007, *ApJ*, 660, L133
- Chernin, L. M., & Masson, C. R. 1995, *ApJ*, 443, 181
- Chibueze, J. O., Imai, H., Tafuya, D., et al. 2012, *ApJ*, 748, 146
- Cunningham, N. J., Moeckel, N., & Bally, J. 2009, *ApJ*, 692, 943
- Curiel, S., Ho, P. T. P., Patel, N. A., et al. 2006, *ApJ*, 638, 878
- Curiel, S., Trinidad, M. A., Cantó, J., et al. 2002, *ApJ*, 564, L35
- Comito, C., Schilke, P., Endesfelder, U., Jiménez-Serra, I., & Martín-Pintado, J. 2007, *A&A*, 469, 207
- Dzib, S., Loinard, L., Rodríguez, L. F., Mioduszewski, A. J., & Torres, R. M. 2011, *ApJ*, 733, 71
- Evans, N. J., II, Slovak, M. H., Becklin, E. E., et al. 1981, *ApJ*, 244, 115
- Hartigan, P., Morse, J., & Bally, J. 2000, *AJ*, 120, 1436
- Hartigan, P., Lada, C. J., Tapia, S., & Stocke, J. 1986, *AJ*, 92, 1155
- Ho, P. T. P., Moran, J. M., & Lo, K. Y. 2004, *ApJ*, 616, L1
- Hiriart, D., Salas, L., & Cruz-González, I. 2004, *AJ*, 128, 2917
- Hughes, V. A., & Wouterloot, J. G. A. 1984, *ApJ*, 276, 204
- Jiménez-Serra, I., Martín-Pintado, J., Caselli, P., et al. 2009, *ApJ*, 703, L157
- Garay, G., Ramirez, S., Rodríguez, L. F., Curiel, S., & Torrelles, J. M. 1996, *ApJ*, 459, 193
- Gómez, J. F., Sargent, A. I., Torrelles, J. M., et al. 1999, *ApJ*, 514, 287
- Gooch, R. 1996, *Astronomical Data Analysis Software and Systems V*, 101, 80
- Goetz, J. A., Pipher, J. L., Forrest, W. J., et al. 1998, *ApJ*, 504, 359
- Narayanan, G., & Walker, C. K. 1996, *ApJ*, 466, 844
- Martín-Pintado, J., Jiménez-Serra, I., Rodríguez-Franco, A., Martín, S., & Thum, C. 2005, *ApJ*, 628, L61
- Moscadelli, L., Reid, M. J., Menten, K. M., et al. 2009, *ApJ*, 693, 406
- Patel, N. A., Curiel, S., Sridharan, T. K., et al. 2005, *Nature*, 437, 109
- Peng, T.-C., Zapata, L. A., Wyrowski, F., Güsten, R., & Menten, K. M. 2012, *A&A*, 544, L19
- Pravdo, S. H., & Tsuboi, Y. 2005, *ApJ*, 626, 272
- Pravdo, S. H., Tsuboi, Y., Uzawa, A., & Ezoe, Y. 2009, *ApJ*, 704, 1495
- Ossenkopf, V., & Henning, T. 1994, *A&A*, 291, 943
- Schneider, P. C., Günther, H. M., & Schmitt, J. H. M. M. 2009, *A&A*, 508, 717
- Schneider, P. C., Günther, H. M., & Schmitt, J. H. M. M. 2009, *A&A*, 508, 321
- Scoville, N. Z., Carlstrom, J. E., Chandler, C. J., et al. 1993, *PASP*, 105, 1482
- Raga, A. C., & Canto, J. 1995, *RMAA*, 31, 51
- Reynolds, S. P. 1986, *ApJ*, 304, 713
- Rodríguez-Franco, A., Martín-Pintado, J., & Wilson, T. L. 1999, *A&A*, 344, L57
- Rodríguez, L. F., Garay, G., Curiel, S., et al. 1994, *ApJ*, 430, L65
- Rodríguez, L. F., Ho, P. T. P., & Moran, J. M. 1980, *ApJ*, 240, L149
- Rodríguez, L. F., Torrelles, J. M., Raga, A. C., et al. 2005, *RMA&A*, 41, 435
- Torrelles, J. M., Verdes-Montenegro, L., Ho, P. T. P., Rodríguez, L. F., & Canto, J. 1993, *ApJ*, 410, 202
- Torrelles, J. M., Patel, N. A., Curiel, S., et al. 2011, *MNRAS*, 410, 627
- Torrelles, J. M., Patel, N. A., Curiel, S., et al. 2007, *ApJ*, 666, L37
- Wilner, D. J., & Welch, W. J. 1994, *ApJ*, 427, 898
- Zapata, L. A., Loinard, L., Su, Y.-N., et al. 2012, *ApJ*, 744, 86
- Zapata, L. A., Schmid-Burgk, J., & Menten, K. M. 2011, *A&A*, 529, A24
- Zapata, L. A., Schmid-Burgk, J., Ho, P. T. P., Rodríguez, L. F., & Menten, K. M. 2009, *ApJ*, 704, L45
- Zapata, L. A., Schmid-Burgk, J., Muders, D., et al. 2010, *A&A*, 510, A2
- Zapata, L. A., Loinard, L., Su, Y.-N., et al. 2012, *ApJ*, 744, 86
- Zapata, L. A., Schmid-Burgk, J., Pérez-Goytia, N., et al. 2013, *ApJ*, 765, L29